Large edge magnetism in oxidized few-layer black phosphorus nanomesh

Yudai Nakanishi[1], Ayumi Ishi[2], Chika Ohata[1], David Soriano[3], Ryo Iwaki[1], Kyoko Nomura[1], Miki Hasegawa[2], Taketomo Nakamura[5], Shingo Katsumoto[5], Stephan Roche[3,4], and Junji Haruyama[1] (✉)

Just Accepted

This is a "Just Accepted" manuscript, which has been examined by the peer-review process and has been accepted for publication. A "Just Accepted" manuscript is published online shortly after its acceptance, which is prior to technical editing and formatting and author proofing. Tsinghua University Press (TUP) provides "Just Accepted" as an optional and free service which allows authors to make their results available to the research community as soon as possible after acceptance. After a manuscript has been technically edited and formatted, it will be removed from the "Just Accepted" Web site and published as an ASAP article. Please note that technical editing may introduce minor changes to the manuscript text and/or graphics which may affect the content, and all legal disclaimers that apply to the journal pertain. In no event shall TUP be held responsible for errors or consequences arising from the use of any information contained in these "Just Accepted" manuscripts. To cite this manuscript please use its Digital Object Identifier (DOI®), which is identical for all formats of publication.

## Large edge magnetism in oxidized few-layer black phosphorus nanomesh

Y. Nakanishi[1], A. Ishii[2], C. Ohata[1], D. Soriano[3], R. Iwaki[1], K. Nomura[1], M. Hasegawa[2], T. Nakamura[5], S. Katsumoto[5], S. Roche[3,4], J. Haruyama[1*]

[1] Faculty of Science and Engineering and [2]Chemistry and Biological Science, Aoyama Gakuin University, 5-10-1 Fuchinobe, Sagamihara, Kanagawa 252-5258, Japan
[3] Catalan Institute of Nanoscience and Nanotechnology (ICN2), CSIC and The Barcelona Institute of Science and Technology, Campus UAB, Bellaterra, 08193 Barcelona, Spain
[4]ICREA—Institució Catalana de Recerca i Estudis Avançats, 08010 Barcelona, Spain
[5] Institute for Solid State Physics, The University of Tokyo, 5-1-5 Kashiwanoha, Kashiwa, Chiba277-8581, Japan
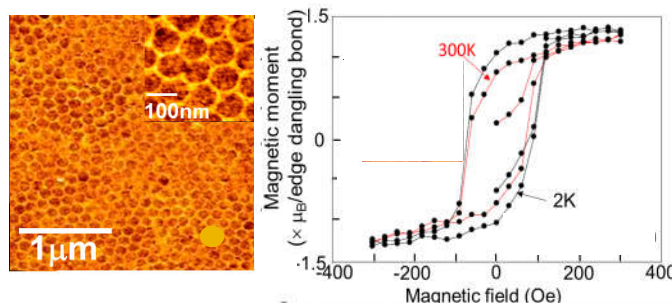
Room-temperature large edge ferromagnetism arises from oxygen(O)-terminated zigzag pore edges of few-layer black phosphorus nanomeshes (BPNMs), which consist of honeycomb like array of hexagonal nanopores formed by a non-lithographic method. The observed magnetization values (per unit area) are ~100 times larger than those reported for hydrogen(H)-terminated graphene NMs, while the magnetism disappears for H-terminated BPNMs. Ferromagnetic spin coupling of edge P=O bond and interlayer spin interaction cause the large magnetism.

*Junji Haruyama, http://www.ee.aoyama.ac.jp/Labs/j-haru-www/

Large edge magnetism in oxidized few-layer black phosphorus nanomesh

Y. Nakanishi[1], A. Ishii[2], C. Ohata[1], D. Soriano[3], R. Iwaki[1], K. Nomura[1], M. Hasegawa[2], T. Nakamura[5], S. Katsumoto[5], S. Roche[3,4], and Junji Haruyama[1] (✉)

[1] *Faculty of Science and Engineering and* [2]*Chemistry and Biological Science, Aoyama Gakuin University, 5-10-1 Fuchinobe, Sagamihara, Kanagawa 252-5258, Japan*
[3] *Catalan Institute of Nanoscience and Nanotechnology (ICN2), CSIC and The Barcelona Institute of Science and Technology, Campus UAB, Bellaterra, 08193 Barcelona, Spain*
[4]*ICREA—Institució Catalana de Recerca i Estudis Avançats, 08010 Barcelona, Spain*
[5]*Institute for solid state physics, The University of Tokyo, 5-1-5 Kashiwanoha, Kashiwa, Chiba 277-8581　Japan*
These authors equally contributed to this work.

KEYWORDS

black phosphorus
nanomesh
edge magnetism
spintronics
zigzag edge
oxygen termination
rare-metal free

ABSTRACT

The formation and control of a room-temperature magnetic order in two-dimensional (2D) materials is a challenging quest for the advent of innovative magnetic- and spintronic-based technologies. To date, edge magnetism in 2D materials has been experimentally observed in hydrogen (H)-terminated graphene nanoribbons (GNRs) and graphene nanomeshes (GNMs), but the measured magnetization remain far too small to allow envisioning practical applications. Herein, we report room-temperature experimental evidences of large edge ferromagnetism (FM) derived from oxygen(O)-terminated zigzag pore edges of few-layer black phosphorus nanomeshes (BPNMs). The magnetization values per unit area are ~100 times larger than those reported for H-terminated GNMs, while the magnetism is absent for H-terminated BPNMs. Magnetization measurements and first-principles simulations suggest that the origin of such magnetic order could stem from a ferromagnetic spin coupling between edge phosphorus (P) with O atoms, resulting in a strong spin localization at edge valence band, and from an uniform oxidation of full pore edges over large area and interlayer spin interaction. Our findings pave the way for realizing high-efficiency 2D flexible magnetic and spintronic devices without the use of rare magnetic elements.

Address correspondence to Junji Haruyama, J-haru@ee.aoyama.c.jp

1 Introduction

Achieving room-temperature long-range magnetic order in atomically thin materials is a key factor to create novel spin functionalities[1-5]. Recently atomic-scale engineering of graphene edges with zigzag-type atomic structure has been shown to give rise to a robust magnetic order[6]. Indeed, high electronic density of states (the so-called edge states) originating from flat energy band of zigzag-edged GNRs, which are one-dimensional (1D) strip lines of graphene, leads to robust spin polarization (i.e., flat-band FM)[7-18]. Flat-band FM has also been demonstrated in H-terminated zigzag-edged GNMs consisting of a honeycomb-like array of hexagonal nano-pores (similar to Fig. 1E), fabricated using a non-lithographic method which enables formation of the low-disordered and low-contaminated pore edges[11-18,36]. Because a GNM roughly corresponds to a large ensemble of zigzag-edged GNRs, small magnetic signals arising from the pore edge spins can be easily detected. Nevertheless to date, the observed magnetization values have been as small as ~10⁻⁶ emu [12,13,36], except for some samples treated by electron beam resist[14].

On the other hand, mono- or few-layer BP have recently been reported as 2D semiconductors with substantial energy band gaps[19,20]. BP has a puckered honeycomb lattice, easily oxidized under air atmosphere exposure, with an in-plane anisotropic atomic structure (i.e., zigzag within monolayer along Y-axis and buckling armchair formed over two layers along X-axis; Fig. 1A)[19-34]. Theoretically, spin polarization arising from edge dangling bonds has been predicted in pristine zigzag-edged phosphorene nanoribbons (ZPNRs) for unrelaxed structures[23]. For the O-terminated case, local edge magnetic moments are predicted to be M_L= 0.27 μ_B for the O atom, 0.39 μ_B for the edge P atom, and 0.13 μ_B for its nearest neighbor. The O-saturated ZPNRs exhibits edge FM due to the spins of unsaturated bonds in weak P=O bonds along the p_z orbitals in the NR plane, whereas H-terminated ZPNRs show no edge FM. This

behavior highly contrasts with that of GNMs[12], in which H-terminated zigzag edges produce flat-band FM while O-terminated edges exhibit diamagnetism. Moreover, stronger and more robust edge anti-ferromagnetism (AFM) (0.155 μ_B for the edge P) has been predicted in ZPNRs due to the electronic instability induced by the half-filled 1D bands, in absence of Peierls transition[27]. To date none of these theoretical results have been confirmed experimentally.

2 Experimental and discussion

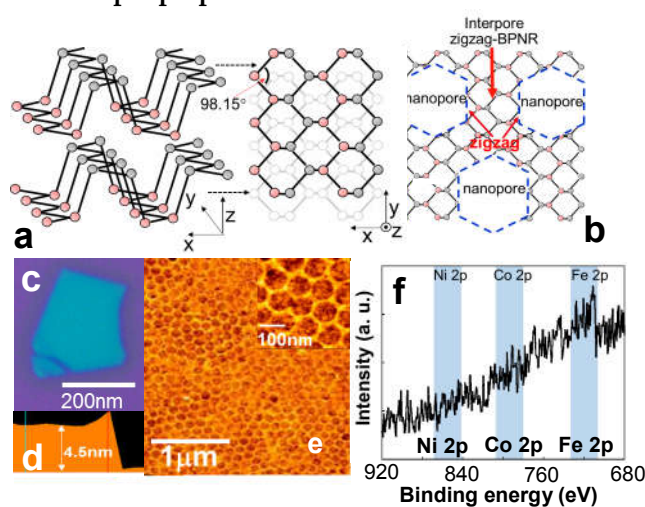### 2.1 Sample preparation and characterization

Figure 1 Structure information of BPNM **(a)** Schematic cross-sectional and top views of a puckered honeycomb lattice of two-layer black phosphorens with AB stacking. Gray and red symbol's P atoms locate within different height. Zigzag edge is within mono layer along y axis, while buckling arm chair edge is formed to z-axis direction along x axis. **(b)** Schematic top view of a BPNM, in which two pore edges are perfectly aligned to zigzag structure. In actual structure, pore size and interpore spacing are much larger and larger number of P atoms exists at the interpore BPNR regions. **(c)** Example of optical microscope image of a flake of few-layer BP mechanically exfoliated from bulk BP. **(d)** Cross-sectional image of (c) obtained using atomic-force microscope. One sample consists of main large flakes and other many small flakes with number of 10~10² (SM 3). Thickness and area of all flakes including small flakes have been measured so as to be 0.1 ~0.4 cm² of the total area with similar thickness (typically ~20nm) in one sample. **(e)** Atomic-force microscope top-view image of a BPNM with hexagonal pores (typical diameter~80nm, interpore distance ~20nm, and pore number~10¹²), which was fabricated via. non-lithographic method (SM1-5) in an extremely careful way (e.g., using plastic tweezers) to avoid incorporating magnetic impurities, defects, and contamination. **Inset:** Higher magnification image. **(f)** XPS spectra of a ferromagnetic BPNM. The binding energies have been calibrated at the Si 2p level in SiO₂ (103.3 eV). 2p₃/₂-binding Energies are 853.8 eV for Ni in

In this work, flakes of few-layered BPs have been mechanically exfoliated from bulk BP (Smart Element Co.) using the Scotch tape method and confirmed using optical (Fig. 1C) and atomic force microscopes (Fig. 1D) (see Supplementary Material (SM) 3). Following the non-lithographic method used to engineer GNMs (i.e, using nano-porous alumina template as an etching mask (SM 1-5)[18]), few-layer BPNMs have been fabricated (Figs.1B and 1E). Interpore regions correspond to BPNRs, but only two edges of each hexagonal pore can be simultaneously perfect zigzag shaped because of the topological constraint of an inner angle of the puckered honeycomb lattice of about ~98.15° (Fig. 1B), which cannot be aligned to the inner angle of the hexagonal pore of 120°. This is different from the case of GNM.

After the formation of nanopore array, the BPNMs have been annealed at a critical temperature (T_c) of 300 °C in a high vacuum (~10^{-6} torr) (SM 6) to favor the formation of zigzag pore edges through edge atomic reconstruction. The absences of any substantial background magnetic impurities and magnetic contamination (e.g., Ni, Fe, Co) have been carefully confirmed by the following methods. First, the XPS measurements of three BPNMs reveal no peaks of typical magnetic orbitals (see Fig. 1F). Second, no magnetic hysteresis loops are observed in two different types of few-layer bulk BP flakes (i.e., without pores), namely in type A (main panel of Fig. 2B), produced using the same fabrication processes as for BPNM (Fig. 2A-sample) without pore formation, and type B (inset of Fig. 2B), in which Ar gas etching process was carried out without using a porous alumina template mask as in the case of BPNM. Third, significant differences between magnetization curves for H and O terminated-BPNMs are observed in Figs. 2A and 2D, which discard the introduction of magnetic impurities introduced during the fabrication process. Finally, the careful fabrication process strongly reduces the presence of magnetic contamination (i.e., bulk BPs mechanically exfoliated by non-magnetic scotch tapes, porous alumina templates fabricated using extremely pure Al substrate (99.99 %) for anodic oxidation, the etching process of BPs for pore formation using Ar gas, and only plastic tweezers have been used

during all the fabrication process). All of these experimental facts can strongly avoid the presence of parasitic magnetic-background. Subsequently, each BPNM has been placed in air atmosphere at 300 K for 2 h, resulting in O-termination of the pore edges, because oxidized top layers serve as protection layers of underneath BP layers preventing their bulk oxidation (SM7). Immediately following this annealing process, magnetization has been measured using superconducting quantum interference devices (Quantum Design Co.).

2.2 Observation of edge magnetisms

Figure 2A shows our main measurement findings of the magnetization of the O-terminated BPNM. Ferromagnetic (FMC)-hysteresis loops are clearly observed with M_s ~ 10^{-4} emu/~0.4 cm². Such M_s value is approximately 100 times larger than those in H-terminated FMC GNMs (i.e., M_s ~ 10^{-6} emu)[12,13]. Importantly, the hysteresis loop at T = 2 K approximately remains unchanged even when increasing the temperature up to T = 300 K. On the other hand, few-layer bulk BP flakes without pores do not exhibit any trace of FMC hysteresis loops (main panel and inset of Fig. 2B). These important results indirectly support that the FM observed in Fig. 2A originates solely from the formation of oxidized nano-pores. This has been confirmed at least in three samples.

Since the oxidation of pore edges is easily obtained by exposing BPNM to air atmosphere, one can assume that all pore edges in a BPNM are O-terminated and can become magnetic. If one assumes that the atomic structure of all the pore edge is zigzag and fully O-terminated, then one can estimate a magnetic moment per edge dangling bond in hexagonal pores in order of ~ 1.0 μ_B, where μ_B is the Bohr magneton (SM 11). This value is in good agreement with our ab-initio simulations of the magnetization value of edge P=O bond as explained later. Accordingly, BP has a significant advantage in which O-terminate edges generate room-temperature magnetism, in contrast with the much smaller FM obtained by partially H-terminated edges in GNM.
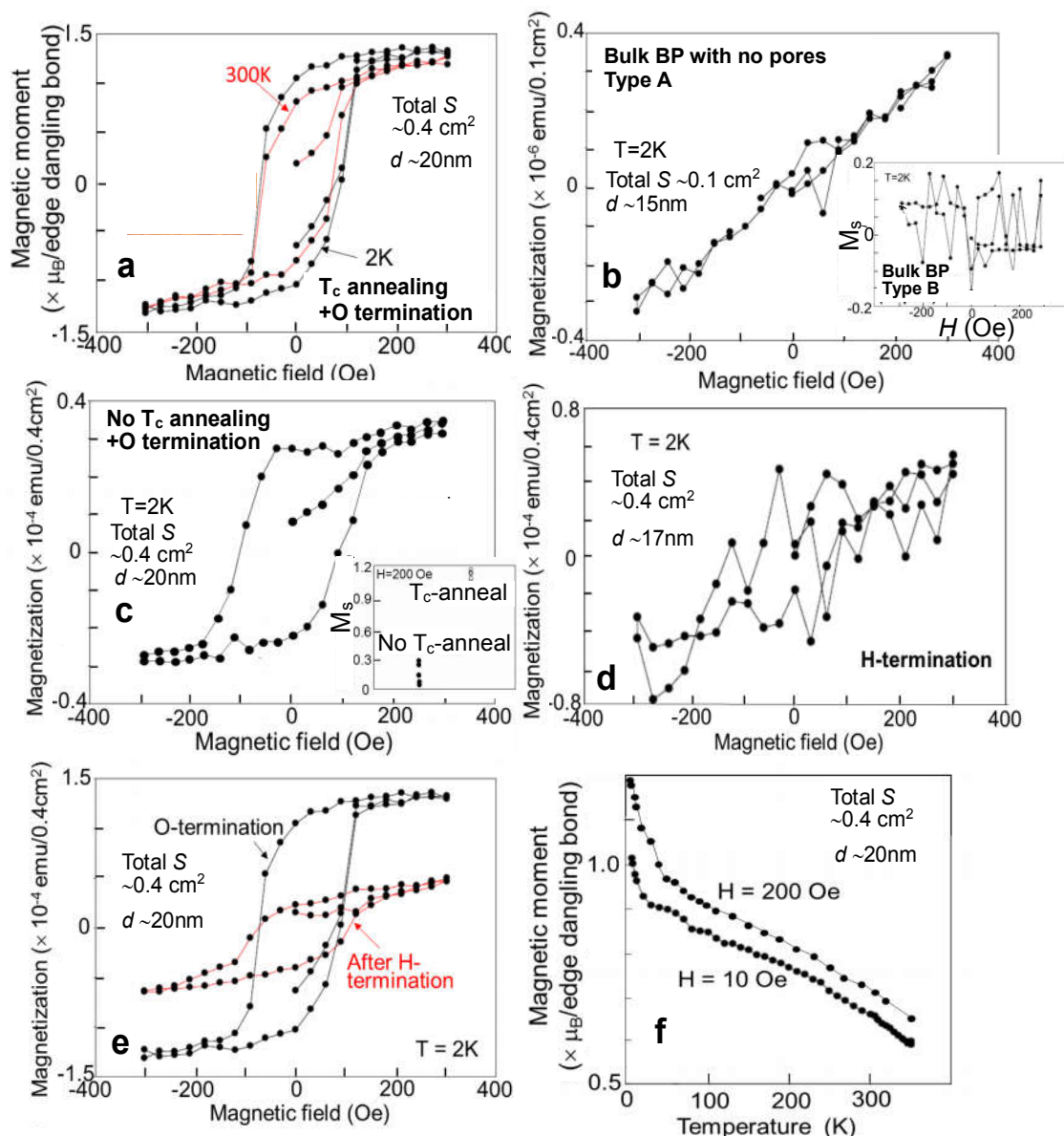
Figure 2 Magnetic measurements of various samples **(a, c-e),** Magnetization curves for BPNMs with **(a)** T_c annealing and O-termination, **(c)** no T_c annealing and O-termination, **(d)** H-termination, **(e)** H-termination of the sample in (a). Y-axis of Figs. 2a and 2f has been normalized by number of O-terminated edge dangling bond of pores (SM 10). **Inset of (c),** Saturation magnetization (M_s) of T_c- and no T_c-annealed BPNMs (each five samples) BPNMs at 2K. Y-axis unit is the same as main panel. **(b)** Magnetization curve for Type-A few-layer bulk BP flake obtained through all the same fabrication process as those for (a)-sample except for the pore formation. **Inset of (b)**; Magnetization for Type-B bulk thick BP, in which Ar gas etching process was carried out without using porous alumina template mask by the same Ar gas condition as that for pore forming. X and Y-axis are the same as main panel. For all samples, no background magnetism was subtracted except for (c), in which a diamagnetic background line was subtracted. S is the sample area including the total pore area. Results of Fig. 2(b) are independent of S. **(f)** Temperature dependence of magnetization values of a magnetic BPNM (i.e., with T_c annealing and O-termination) measured with decreasing temperatures.

Figure 2C reveals that the non-annealed BPNM exhibit FMC hysteresis loops with M_s about 4 times lower than those of the T_c-annealed samples (i.e., Fig. 2A). Such result implies that annealing at the T_c is important for introducing large FM. Indeed, reproducibility of magnetism in non-annealed BPNMs is poor with some samples showing M_s values smaller than ~0.3 ×10⁻⁴ emu/100 μm² (inset of

Fig. 2C). In the case of FMC GNMs, the zigzag-type edge atomic structure is the most stable structure from both thermal and chemical perspectives[12,16-18], hence annealing at the T_c result in the formation of zigzag pore edges and the subsequent formation of FM after H-termination. The occurrence of similar pore-edge atomic reconstruction to a zigzag geometry is also expected for the pores of our BPNMs (Fig. 1B) following annealing at the T_c, leading to FM after O-termination (Fig. 2A). This is supported by Raman spectroscopy as discussed below.

Figure 2D shows the magnetization curve for the BPNM obtained after annealing under an H_2 atmosphere at 300 °C during 2 h immediately after the formation of nanopores. In contrast to the O-terminated BPNM, the H-terminated BPNM barely exhibit a FMC-hysteresis loop and the magnetic signal is paramagnetic and noisy. This has been confirmed at least in four samples. Moreover, the M_s of an O-terminated sample subsequently annealed under an H_2 atmosphere at T_c ~ 300 °C for 5 h (Fig. 2E) is ~3 times smaller than that of the original O-terminated sample (Fig.2A). The disappearance of FM in the H-terminated BPNM is consistent with the theoretical prediction of the absence of FM in PNRs with H-terminated zigzag edges s mentioned in introduction. In particular, the result in Fig. 2E suggests that O-termination of the zigzag pore edges is highly stable and cannot be entirely replaced by H-termination.

Temperature-dependence of M_s and magnetization close to residual magnetization (M_r) are shown in Fig. 2F (SM 10). Both M values monotonically increase with decreasing temperature (e.g., from ~0.65 × 10^{-4} emu/0.4 cm^2 (300K) to ~1.0 × 10^{-4} emu/0.4 cm^2 (2K) for H = 10 Oe and ~0.7 (300K) to ~1.2 (2K) for H = 200 Oe). Hence, the difference of M_s and M_r between 2K and 300K is evident. This result definitely reinforces the origin of the FMC hysteresis loops observed at 2K and 300K in our O-terminated BPNMs. We finally note that the expected Curie temperature of measured FMC BPNMs should be above 350℃, which is the upper limit temperature of our SQUID.
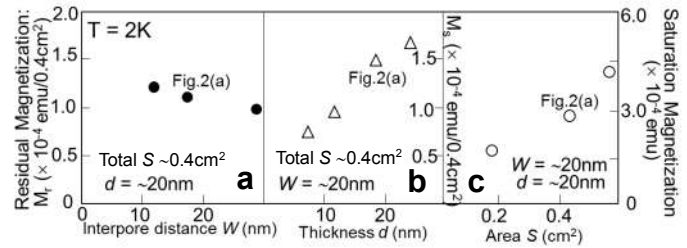

Figure 3 Structure dependence of magnetisms **(a)** Residual magnetization (M_r) of FMC BPNMs as a function of the interpore distance (W) (i.e., width of the interpore PNR regions), and M_s as a function of the **(b)** thickness (d) and **(c)** sample area (S). Values of Fig.2(a)-sample are noted on individual figures. W has been controlled by that in porous alumina template mask formed by changing temperature of anodic oxidation of Al substrate e.g., (0 ~ 10℃). In contrast, samples with different d and S have been selected from many random samples.

Figure 3 gives M_r of the FMC-BPNMs (i.e., O-terminated BPNMs) as a function of the interpore distance (W), which is identical to the width of an interpore BPNR, and M_s as a function of the thickness (d) and sample area (S). The M_r value appears to be not very sensitive to W, despite a very weak decay with increasing W owing to lower pore density (Fig. 3A; W has been changed with keeping a constant pore diameter), which is consistent with previous theories of ZPNRs[23,27] and with our theoretical simulations described below. This also suggests that the oxidation of the interpore bulk BP regions is not dominant for the observed FM[31]. Indeed, if the formation of bulk magnetic phase would be dominant, M_r should manifest larger increase when varying W from 10 to 30 nm (under a constant pore diameter and sample area), following the threefold increase of the area of interpore bulk phase region, while the total number of hexagonal cell per the sample area decreases in 9/11 (i.e., area of one hexagonal cell consists of a pore diameter 80 nm+ half of W, corresponding to 90 nm diameter for W = 10nm and 110nm diameter for W = 30nm). This cannot explain the very low variation of M_r shown in Fig.3a.

We also remark that this M_r behavior contrasts with that in the flat band FM observed in H-terminated GNMs, for which the Coulomb exchange interaction between two opposite edges of the interpore GNRs strongly decays with increasing W, leading to a loss of the stability of the FMC spin ordering and hence a lower M_r[21]. The reason for this difference is related to the edge P=O

bonds and is further explained in the theoretical section. On the other hand, M_s is seen to scale linearly with d and S (Figs. 3B and 3C), but the dependence on d suggests that M_s becomes negligible in the BPNM mono-layer limit. This could be explained by the strong interlayer interactions in AB stacking of BP (Fig. 1A), favoring the FMC spin configuration, similarly to the case of graphene[25].

Our theoretical calculations for ZPNR actually support this result and also indicate even much stronger interlayer interaction as explained later (Figs. 6E and 6F). This interlayer spin interaction makes long-range spin ordering stable even at 300 K (Fig. 2A). The linear dependence on S (Fig. 3C) arises because the area of the O-terminated zigzag pore edges linearly increases with S. This means that the fully O-terminated pore edges uniformly exist through all layers in individual samples. This implies that the O-termination of the pore edges of BPNMs can be easily realized only by exposing samples to air atmosphere and significantly contributes to the observed large-magnitude edge magnetism. Additionally, as discussed above, annealing at T_c may cause the reconstruction of the pore-edge atomic structure, resulting in formation of zigzag pore edges and subsequent formation of FM after O-termination. Because the BPNM tends to disappear when annealing at T > 350 °C, the annealing temperature of 300 °C is approximately the critical temperature T_c at which the reconstruction of pore-edge atomic structures takes place in BPNMs. In comparison, this T_c is much lower than ~800 °C for the FMC GNMs.

2.3 Raman spectrum and pore edge atomic structures

The analysis of typical Raman spectra of O-terminated BPNMs, exhibiting FMC or non-FMC signals, provide further support to the above

Figure 4 Raman measurement of BPNMs **(a)** Typical micro Raman spectra for two O-terminated BPNMs that do and do not exhibit FM. Both samples have been fabricated by the same process. **(b)** Correlation of the d and I_{Ag1}/I_{Si} values in the Raman spectra measured in the bulk and at the edges of three few-layer BP flakes (i.e., without nanopores) without T_c annealing. The linear dotted lines indicate trends for the individual correlations. The I_{Ag1}/I_{Si} values for the FM (○)

and non FM (×) BPNMs, including the result of Fig. 4(a), are also noted. **Inset:** Example of Raman mapping for sample BP4 in main panel. Red, orange, and yellow symbols mean the measured points with results of $I_{Ag1}/I_{Si} > 0.5$, $0.5 > I_{Ag1}/I_{Si} > 0.3$, $0.3 > I_{Ag1}/I_{Si}$, respectively.
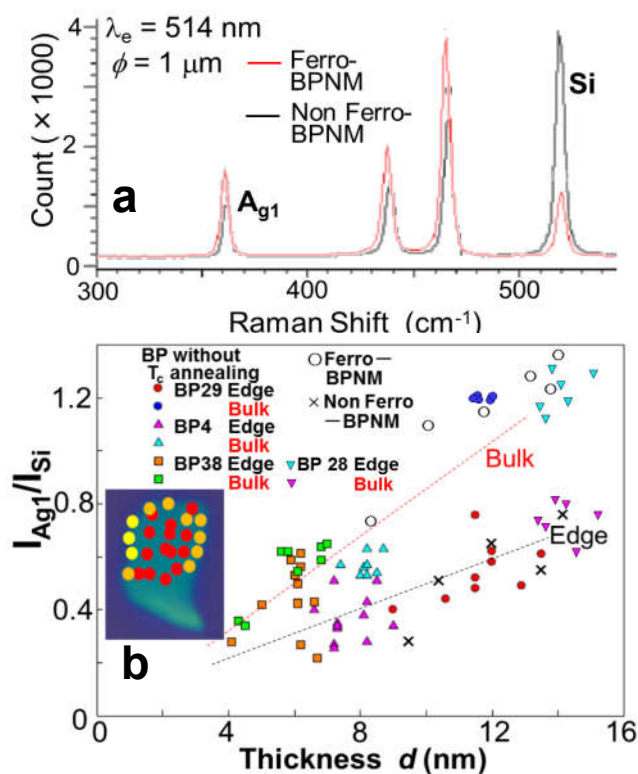
argument about pore edge atomic structures (Fig. 4A; SM 8). From Fig. 4A, it is confirmed that the heights of the band peaks due to the phonons resulting from interlayer interactions (I_{Ag1}) are nearly the same in the spectra of the two samples, while the intensity of the band attributed to the phonon from the Si substrate (I_{Si}) is significantly larger in the non-FMC sample, leading to a low I_{Ag1}/I_{Si} value. We find that this tendency agrees with that from the bulk regions and edges of few-layer BP flakes (i.e., without nano-pores) of different d not annealed at T_c (Fig. 4B). Fig. 4B implies that the I_{Ag1}/I_{Si} ratios observed at the edges are lower than those of the corresponding bulk regions in nearly all of the samples (Inset), and an approximately linear correlation between the I_{Ag1}/I_{Si} ratio and d is obtained[22]. The lower I_{Ag1}/I_{Si} values at the edges can be obtained from the same relationship as that in Fig. 4A (i.e., the higher peak value of I_{Si}). Indeed, the I_{Ag1}/I_{Si} values for the FMC (○) and non-FMC (×) BPNMs,

including those shown in Fig. 4A, follow the peak trends for the bulk regions and edges plotted in Fig. 4B, respectively.

The lower I_{Ag1}/I_{Si} values at the edges of BP flakes can be attributed to the following two possibilities; namely (1) the presence of the buckling armchair-rich edges or (2) the influence of the scattered laser beams from the Si substrate. The possibility (1) originates from the following two reasons. First, since the BP flakes without nano-pores were just mechanically exfoliated from bulk BP without any intentional alignment of crystal axis and not by annealing at the T_c, the edge atomic structures should be rough edges but preferentially of buckling armchair type. This is because zigzag edge appears only when crystal axis is perfectly aligned along Y axis in Fig. 1A, while in any other cases the buckling armchair edge appears. Second, the intensity of the phonons from the Si substrate beneath the buckling armchair edges is higher than that of phonons at the zigzag edges, because the buckling armchair structures are formed along z-axis (i.e., along out-of-BP plane; Fig. 1A) and the surface of the Si substrate can easily oscillate under them (e.g., beneath gray P atoms). Indeed, the phonon dispersion along the zigzag direction was shown to be sharper than that along the buckling armchair direction using first-principles calculations for BP[26]. However, these effects are suppressed in the bulk region in few layer BPs and, hence, the I_{Ag1}/I_{Si} values are not high. On the other hand, all phonons are more effectively activated at sample edges than in the bulk regions. This effect should be more significant for phonon arising from Si substrate under the buckling armchair structure for the abovementioned reasons.

On the other hand, the possibility (2) directly results in high I_{Si} signals. As mentioned above, the I_{Ag1}/I_{Si} values for the FMC and non-FMC BPNMs follow the peak trends for the bulk regions and edges plotted in Fig. 4B. Because the pore structures (i.e., diameter and hexagonal shape) observed by SEM and atomic force microscope are almost the same in these two-type BPNMs, the contribution of such possibility (2) should be also the same. This cannot explain different I_{Si} in Fig. 5. Therefore, possibility (1) is the origin for Fig. 4.

Hence, the low I_{Ag1}/I_{Si} ratios arising from the high I_{Si} values in Fig. 4A suggest the buckling armchair-rich pore edges in the non-FMC BPNM. In contrast, it can be concluded that the pore edge of the FMC BPNMs is zigzag rich, resulting from edge reconstruction during annealing at T_c. This also suggests the formation of partial zigzag edges in other pore edges in addition to the two zigzag pore edges (inset of Fig. 2A) (SM 9). Only two out of ten BPNMs did not result in zigzag-rich pore edges after annealing at T_c (SM 9). This also suggests that the buckling armchair edge requires higher energy for stability after the T_c annealing and therefore is hard to be realized. The reconstruction by the T_c annealing may introduce relaxed structure to interpore BPNRs, which conventionally results in Peierls transition and disappearance of magnetism[24,27]. However, the present BPNM structure, in which six BPNRs with a typical width ~20nm form one hexagonal unit cell leaving a nanopore at the center, may prevent occurrence of Peierls transition.

2.4 Theoretical analysis

We now theoretically investigate the presence of edge-magnetism in O-terminated ZPNRs by performing first principles calculations (SM 12). Figure 5A shows the band structure of the relaxed O-terminated 10-ZPNRs (Fig. 5B) considered in our calculations. The left and right panels correspond to the spin-unpolarized and -polarized cases, respectively. Similarly to previous calculations, a pair of midgap states (red arrow in Fig.5A) span across the band gap and cross the Fermi level at around π/2a of the Brillouin zone (BZ) inducing a metallic state. The midgap states at Γ and X (right panel of Fig. 5A) are completely localized along the edges as seen in Figs.5B and 5C. This is related to the small band splitting observed at the -point for O-terminated PNRs, which is much smaller than Ref. 24, and implies a strong reduction of inter-edge coupling in presence of O. This is in agreement with Fig.3A.
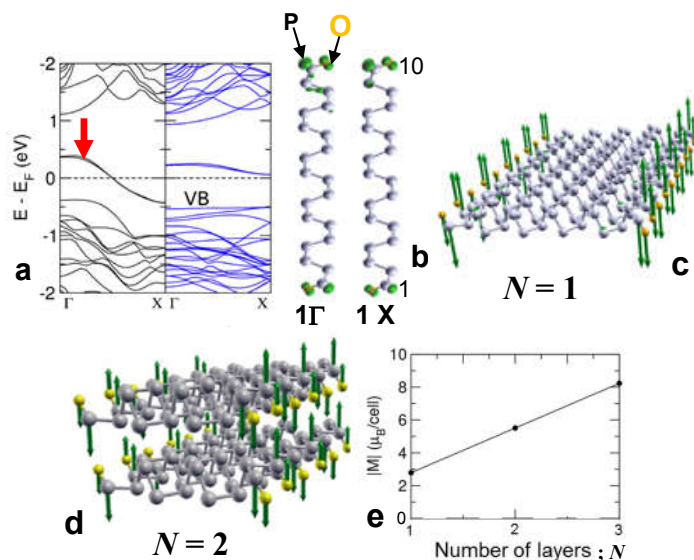
Figure 5 First principles calculations of zigzag PNR(ZPNR) **(a)** Band structures for O-terminated 10-ZPNR. Left and right panels correspond to spin-unpolarized and -polarized cases (SM11). **(b)** Charge density contribution (shown in green) of one of the midgap states (red arrow in (a)) at Γ and X. The structure corresponds to O-terminated interpore ZPNR region of BPNM. Distances are very similar to those reported for mono-layer PNR. The distance between P and O atoms at the edges is 1.5 Å, which corresponds to a P=O double bond. **(c, d)** Illustration of the edge anti-FM emerging at **(c)** the mono-layer zigzag edges corresponding to (b) and **(d)** the bi-layers. Green arrows correspond to the spin magnetic moment computed on each atom. **(e)** Scaling of the absolute magnetization per unit cell with number of layers (N). Relaxed interlayer-distance ($d_z \approx 0.198$ nm) is around 0.1 nm shorter than previously report.

We have also checked inter-edge magnetic coupling for both parallel and antiparallel couplings of edge-FMC and edge-Anti-FMC (AFMC) configurations in the doubly relaxed unit cells. We found that the total energies were very similar ($\Delta E < 1$ meV), which highlights the small spin interaction between edges. The edge-FMC configuration with antiparallel inter-edge coupling (similar to zigzag GNRs) always led to non-magnetic or bad converged solutions. In contrast, the edge-AFMC configuration always converged very fast while keeping the initial AFMC guess along the edge. Interestingly, the O atoms were not initially polarized and became magnetic during the self-consistency calculation. The magnetic moments emerging at the O atoms couple ferromagnetically with the ones at the neighboring P_{edge} atoms giving rise to a huge enhancement of the edge magnetism (the green arrows in Fig. 5C; SM 12). The values of the local

magnetic moment M_L at the P_{edge} and O atoms for the O-terminated 10-ZPNR are $|M_P| = 0.55$ μ_B and $|M_O| = 0.4$ μ_B, respectively (very similar to the O-terminated 6-ZPNR). The calculated total M_L is around 1 μ_B per P=O dimer, almost seven times bigger than those in Ref 27. We also reveal that at the X-point the spin densities from the valence bands are only localized along the edges of the NR which strongly contributes to the edge-Anti-FMC state (SM 11). Although the M_L value is only a few times larger than that of the FMC GNMs ($M_L \sim 0.2$ or 0.3 μ_B)[12], the uniform oxidation of pore edges through all layers in a BPNM allows this large magnetism. Since the H-termination eliminates the abovementioned unsaturated bond, magnetism disappears.

Interlayer edge-spin coupling in the O-terminated ZPNRs also strongly contributes to the FM as shown in Figs. 5C and 5D (SM 11). Misalignment of interlayer adjacent O=P_{edge} atoms in AB stacking allows FMC spin configuration in bilayer ZPNRs (Fig. 5C) as well as the case of few-layer GNRs. However, the strong interlayer interaction due to the O atom (SM 12) induces this FMC spin alignment and makes spin ordering more stable. Indeed, the linear scaling of the absolute magnetization, defined as the sum of the absolute values of the M_L (m_i) on each atom, $|M| = \Sigma_i |m_i|$, is confirmed with the number of layers (N) as shown in Fig.5D. This is qualitatively consistent with Fig. 3B.

3 Conclusions

In conclusion, our results suggest the formation of room-temperature pore-edge FM in O-terminated BPNMs that is ~100 times/area larger than that reported for FMC GNMs. In contrast to H-terminated GNMs where edge hydrogenation is delicate under H_2 atmosphere and not very stable, O-termination of BPNMs is robust in air atmosphere. Moreover, while O-termination suppresses magnetization in GNMs, oxidation enhances edge magnetism in BPNMs. Therefore, the emergence of magnetization with O-termination should be significantly advantageous compared to the H-termination in GNMs for the generation of edge magnetism in low-dimensional materials. Experimental results

are supported by first principles calculations which suggest that the FMC spin coupling of edge P atom with O atom existing for large sample area and the strong spin localization of edge valence band could be at the origin of large edge magnetism. Besides, interlayer spin interaction induces this FMC spin alignment and makes spin ordering stable. On the other hand, the fact that M_r is not very sensitive to *W* sharply differs from the case of H-terminated GNMst and is theoretically understood from weak edge-spin interaction of FMC-coupled edge P=O bonds in O-terminated BPNRs.

Edge magnetism in molybdenum disulfide (MoS_2) was also reported[35]. However, it was much different from the present case. For example, FMC hysteresis loop of the result was not evident in the work. Moreover, the M-H curves provided a component of the large diamagnetism background signal. Consequently, these results differ substantially from having a large hysteresis loop with less diamagnetic background, as in our study. Furthermore, in our work the formation of the FMC state can be tuned by a different type of chemical treatment (using O- or H-termination), acting preferentially on the pores edges. This is difficult in MoS_2. Very recently, we have revealed edge FM in O-terminated hexagonal boron-nitride (hBN) and its elimination in H-terminated sample[37]. Although the results was qualitatively similar to the present case, amplitude of the observed FM was very small because only the edge N=O bond yielded the FM.

The formation and the control of a room temperature magnetic order in 2D materials stand as genuine milestones, and our reported realization of room-temperature FM (without using rare-earth magnetic atoms) in oxidized-BPNMs is therefore highly valuable for the development of future innovative magnetic- and spintronic-based technologies.

Acknowledgements

Electronic Supplementary Material: Supplementary material (e.g., further details of the sample preparation methods, other measurement results) is available in the online version of this article at http://dx.doi.org/10.1007/s12274-***-****-* (automatically inserted by the publisher).

References

[1] Ferrari, A. C.; Novoselov, K. S.; Roche, S. *et al.,* Science and technology roadmap for graphene, related two-dimensional crystals, and hybrid systems. *Nanoscale*, 2015, **7**, 4587.

[2] Roche, S.; Fert. A. *et al.,* Graphene spintronics: the European Flagship perspective. *2D Materials,* 2015, **2**, 030202.

[3] Yang, H. X.; Hallal, A.; Terrade, D.; Waintal, X.; Roche, S.; and M. Chshiev Proximity effects induced in graphene by magnetic insulators: First-principles calculations on spin filtering and exchange-splitting gaps. *Phys. Rev. Lett.* 2013. **110**, 046603; Leutenantsmeyer, J. C.; Kaverzin, A. A; Wojtaszek, M.; van Wees, B. J. Proximity induced room temperature ferromagnetism in graphene probed with spin currents . *2D Materials,* 2017, **4**, 014001.

[4] Avsar, A. *et al.,* Spin–orbit proximity effect in graphene. *Nature Com*m. 2014, **5**, 4875.

[5] Lin, C. *et al.,* Direct Observation of ordered configurations of hydrogen adatoms on graphene. *Nano Lett*. 2015, **15**, 903.

[6] Magda, G. Z.; Jin. X.; Hagymási, I.; Vancsó, P.; Osváth, Z.; Nemes-Incze, P.; Hwang, C.; Biró, L. P.; Tapasztó L. Room-temperature magnetic order on zigzag edges of narrow graphene nanoribbons. *Nature,* 2014, **514**, 608.

[7] Nakada, K.; Fujita, M.; Dresselhaus, G.; and Dresselhaus, M. S. Edge state in graphene ribbons: Nanometer size

effect and edge shape dependence. *Phys. Rev. B.* 1996, **54,** 17954.

[8] Soriano, D.; Leconte, N.; Ordejón, P.; Charlier, J. C.; Palacios, J. J.; and Roche, S. Magnetoresistance and Magnetic Ordering Fingerprints in Hydrogenated Graphene. *Phys. Rev. Lett.* 2011, **107**, 016602.

[9] Lee, H.; Park, N.; Son, Y. W.; Han, S.; Yu, J. Ferromagnetism at the edges of the stacked graphitic fragments: an ab initio study. *Chem. Phys. Lett.* 2004, **398**, 207.

[10] Kusakabe, K.; Maruyama, M. Magnetic nanographite. *Phys. Rev. B.* 2003, **67**, 092406.

[11] Shimizu, T.; Haruyama, J.; Marcano, D. C.; Kosinkin, D. V.; Tour, J. M.; Hirose, K.; Suenaga, K. Large intrinsic energy bandgaps in annealed nanotube-derived graphene nanoribbons. *Nature Nanotech.* 2011, **6,** 45.

[12] Tada, K.; Hashimoto, T.; Haruyama, J.; Yang, H.; Chshiev, M. Spontaneous spin polarization and spin pumping effect at edges of graphene antidot lattices. *Phys. Status Solidi B.* 2012, **249**, 2491.

[13] Kato, T.; Nakamura, T.; Kamijyo, J.; Kobayashi, T; Yagi, Y.; Haruyama, J. High-Efficiency graphene nanomesh magnets realized by controlling hydrogenation of pore edges. *Appl. Phys. Lett.* 2014, **104**, 252410.

[14] Hashimoto, T.; Kamikawa, S.; Haruyama, J.; Soriano, D.; Pedersen, J. G.; Roche, S. Tunneling magnetoresistance phenomena utilizing graphene magnet electrodes. *Appl. Phys. Lett.* 2014, **105**, 183111.

[15] Hashimoto, T.; Kamikwa, S.; Yagi, Y.; Haruyama, J. Electronic properties of nanopore edges of ferromagnetic graphene nnomeshs at high carrier densities under ionic-liquid gating. *Mat. Sciences and Appl.* 2014, **5(1)**, 1.

[16] Jia, X.; Dresselhaus, M. S. *et al.,* Controlled formation of sharp zigzag and armchair edges in graphitic nanoribbons. *Science.* 2009, **323**, 1701.

[17] Girit, C. O.; Zettl, A. *et al.,* Graphene at the edge: Stability and dynamics. *Science.* 2009, **323**, 1705.

[18] You, Y.; Ni, Z.; Yu, T.; and Shen, Z. Edge chirality determination of graphene by Raman spectroscopy. *Appl. Phys. Lett.* 2008, **93,** 163112.

[19] Li, L.; Yu, Y.; Ye, G. J.; Ge, Q.; Ou, X.; Wu, H.; Feng, D.; Chen, X. H.; Zhang, Y. Black phosphorus field-effect transistors. *Nature Nanotech.* 2014, **9**, 372.

[20] Churchill, H. O. H.; Herrero, P.-J. Phosphorus joins the family. *Nature Nanotech.* 2014, **9**, 330.

[21] Koenig, S. P.; Doganov, R. A.; Schmidt, H.; Castro Neto, A. H.; Özyilmaz, B *et al.,* Electric field effect in ultrathin black phosphorus. *Appl. Phys. Lett.* 2014, **104**, 103106.

[22] Gomez, A. C. *et al.,* Isolation and characterization of few-layer black phosphorus. *2D Materials* 2014, **1**, 025001.

[23] Zhu, Z.; Li, C.; Yu, W.; Changi, D.; Sun, Q.; Jia, Y. Magnetism of zigzag edge phosphorene nanoribbons. *Appl. Phys. Lett.* 2014, **105**, 113105.

[24] Peng, X.; Copple, A.; Wei, Q. Edge effects on the electronic properties of phosphorene nanoribbons. *J. Appl. Phys*. 2014, **116**, 144301.

[25] Carvalho, A.; Rodin, A. S.; and Castro Neto, A. H. Phosphorene nanoribbons. *Euro. Phys. Lett.* 2014, **108**, 47005.

[26] Ong, Z. Y.; Cai, Y.; Zhang, G.; Zhang, Y. −W. Strong thermal transport anisotropy and strain modulation in single-layer phosphorene. *J. Phys. Chem. C.* 2014, **118**, 25272.

[27] Du, Y.; Liu, H.; Xu, B.; Sheng, L.; Yin, J.; Duan, C. G.; Wan, X. Unexpected magnetic semiconductor behavior in zigzag phosphorene nanoribbons driven by half-filled one dimensional band. *Sci. Rep.* 2015, **5**, 8921.

[28] Zhu, W.; Yogeesh, M. N.; Yang, S.; Aldave, S. H.; Kim, J-S.; Sonde, S.; Tao, L.; Lu, N.; Akinwande, D. Black phosphorus radio-frequency transistors. *Nano Lett.* 2015, **15**, 1883.

[29] Dai, J.; Zeng, X. C., Bilayer phosphorene: effect of stacking order on bandgap and its potential applications in thin-film solar cells. *J. Phys. Chem. Lett.* 2014, **5**, 1289.

[30] Luo, X.; Lu, X.; Koon, G. K. Y.; Castro Neto, A. H.; Özyilmaz, B.; Xiong, Q.; Quek, S. Y. Large Frequency Change with Thickness in Interlayer Breathing Mode —Significant Interlayer Interactions in Few Layer Black Phosphorus. *Nano Letters.* 2015, **15**, 3931.

[31] Ziletti, A.; Carvalho, A,; Trevisanutto, P. E.; Campbell, D. K.; Coker, D. F.; Castro Neto, A. H. Phosphorene oxides: Bandgap engineering of phosphorene by oxidation. *Phys. Rev. B.* 2015, **91**, 085407.

[32] Liu, H.; Neal, A. T.; Zhu, Z.; Luo, Z.; Xu, X.; Tománek, D.; Ye, P. D. Phosphorene: an unexplored 2D semiconductor with a high hole mobility. *ACS Nano.* 2014, **8** (4), 4033.

[33] Gillgren, N. *et al.,* Gate tunable quantum oscillations in air-stable and high mobility few-layer phosphorene heterostructures. *2D Mater.* 2015, **2** (1), 011001.

[34] Zhu, Z.; Tomanek, D., Semiconducting Layered Blue Phosphorus: A Computational Study. *Phys. Rev. Lett.* 2014, **112** (17), 176802.

[35] Tongay, S.; Varnoosfaderani, S. S.; Appleton, B. R.; Wu, J.; Hebard, A. F. Magnetic properties of MoS_2: Existence of ferromagnetism. *Appl. Phys. Lett.* 2012, **101**, 123105.

[36] Haruyama, J. Graphene and Graphene Nanomesh Spintronics. *Special Issue on "Carbon Nanoelectronics" in Electronics*, **2013**, **2**(4), 368.

[37] Ohata., C.; Tagami, R.; Nomura, K.; Haruyama, J. Hexagonal boron-nitride nanomesh magnets, *Appl. Phys. Lett.* 2016, **109**, 133110.

Electronic Supplementary Material

Large edge magnetism in oxidized few-layer black phosphorus nanomesh

Y. Nakanishi[1], A. Ishii[2], C. Ohata[1], D. Soriano[3], R. Iwaki[1], K. Nomura[1], M. Hasegawa[2], T. Nakamura[5], S. Katsumoto[5], S. Roche[3,4], and Junji Haruyama[1] (✉)

[1] Faculty of Science and Engineering and [2]Chemistry and Biological Science, Aoyama Gakuin University, 5-10-1 Fuchinobe, Sagamihara, Kanagawa 252-5258, Japan
[3] Catalan Institute of Nanoscience and Nanotechnology (ICN2), CSIC and The Barcelona Institute of Science and Technology, Campus UAB, Bellaterra, 08193 Barcelona, Spain
[4]ICREA—Institució Catalana de Recerca i Estudis Avançats, 08010 Barcelona, Spain
[5]Institute for solid state physics, The University of Tokyo, 5-1-5 Kashiwanoha, Kashiwa, Chiba 277-8581　Japan

(1) Fabrication of nano-porous alumina template (NPAT) masks

The NPAT, which consists of a honeycomb array of hexagonal-shaped nanopores (Fig. S1a,b), was fabricated by the anodic oxidation of a pure aluminum (Al) substrate (Al = 99.99%) using electrochemical methods with a carbon electrode as the cathode. Due to self-organization, a NPAT provides structure parameters (e.g., pore diameter ϕ and interpore space w) with exceptionally high regularity and high reproducibility. After the formation, the NPAT with an area of about 1 cm² was detached from the Al substrate by alternating the polarity of the two electrodes. The detached NPATs were then placed onto the BPs on Si(SiO₂) substrate as etching masks (Supplementary material (SM) (4) as below). SQUID measurements prove
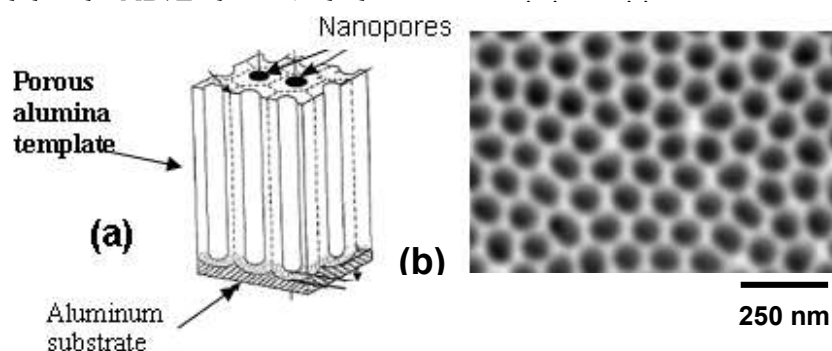

Fig. S1. (a) Schematic view of porous alumina template mask. **(b)** SEM top view of (a).

(2) Two advantages of the nonlithographic fabrication method of BPNMs

The advantages of using the NPAT mask in conjunction with low-power gas etching (SM (4)) and the T_c annealing (SM (6) below) can be explained as follows:

① Because this process uses the nonlithographic fabrication method, it ensures minimal magnetic defects and magnetic contamination to the nanopore edges.
② The honeycomb-like hexagonal nanopore array can result in the formation of a large number of BPNRs

with sufficient lengths (e.g., 40 nm in the present case) because of the presence of six boundaries among the neighboring six pores compared with that of lattices of the square- and round-shaped pores. In the actual BPNM, it is speculated that zigzag and armchair edges may exist with mixed states in one BPNR (one boundary), as confirmed by the AFM observation. Even in this case,

③ A large number of BPNRs in the present BPNM s can yield a large area of assembled zigzag-edge BPNRs.

(3) Fabrication of bulk few-layer black phosphorus

The few-layer BP samples as the base for formation of BPNMs were extracted from bulk BP (Smart Element Co.) onto degenerately doped Si wafers with almost no SiO_2 surface layer by means of mechanical exfoliation using scotch tape. Optical microscope, Raman spectroscopy, and cross-correlation with an AFM profile allowed us to identify the number of deposited BP layers.
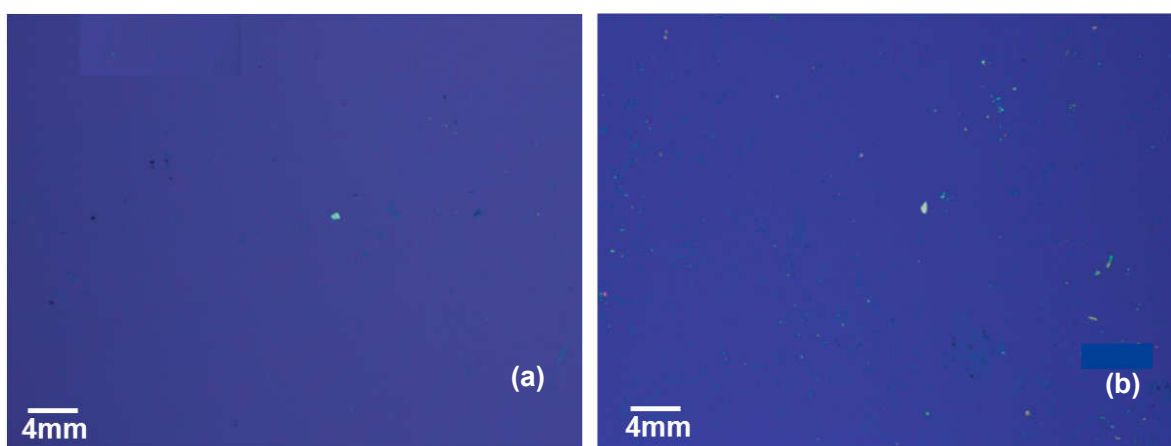

Fig. S2: Typical low magnification micrographs of BP samples after small flakes were manually removed. **(a)** Sample in which almost small flakes could be removed, remaining only one large BP flake. **(b)** Sample in which many small flakes still remained even after removal, because it had many flakes as exfoliated and it was difficult to manually remove all small flakes, remaining the main large flake without giving damage.

Two typical examples of low magnification micrographs are shown in Fig. S2. We have tried to remove unwanted small flakes by plastic tweezers as much as possible. In (a), only a large main flake is basically observed, because amount of unwanted small flakes was small as exfoliated. In contrast, in (b), it was difficult to remove all small flakes, maintaining the main large flake without giving damages, because amount of small flakes was large as exfoliated.

However, we have carefully checked thickness and area of all flakes including small flakes (number of $10 \sim 10^2$) so as to be 0.1 ~0.4 cm^2 of the total BPNM area with similar thickness in one sample.

(4) Formation of nanomesh on few-layer BPs using NPAT masks: development of new attaching method

Using the NPAT explained in SM (1) as a mask, assembled BPs explained in SM (3) were etched by a carefully optimized low-power Ar gas (e.g., 200–600 V for 10 – 40 min) to avoid giving magnetic defects. In order to realize accurate etching of the BP, it is indispensable to attach the NPAT mask highly close to the BP surface. We developed new method to confirm this by checking the color of NPAT/BP surface by optical microscope. We found that they are the most close when the colors looks rainbow like Fig. S3(b).
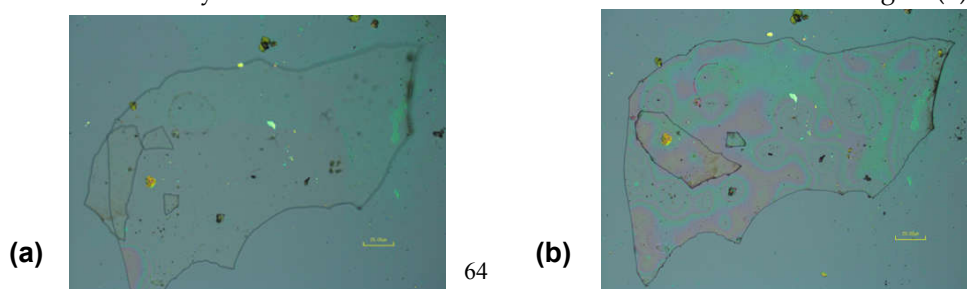
Fig. S3. Optical micro scope images of examples of NPAT on BP **(a)** with poor attachment and **(b)** close attachment.

Then, we carried out the low-power etching step by step. Each after etching in 10 minutes, we performed FESEM (or AFM) observation and checked formation of nanomesh on Si-substrate under the NPAT mask. Until confirmation of formation of the nanomesh on Si-substrate, we repeated the slight etching. This is very important process to avoid giving magnetic defects to the pore edges.

Ar gas etching gives damage (defects) to the crystals more or less. However, this low amount of defects is recovered by T_c annealing. We carefully optimized condition for low-power Ar gas etching to reduce magnetic defects as much as possible, when we fabricated ferromagnetic GNM in our past works. In the case of graphene, amount of the defects is easily confirmed by observing D peak height in Raman spectrum. Indeed, we realized almost zero peak height and zero defects, using the best etching condition and the T_c annealing. In contrast, it is difficult to clearly confirm amount of defects from Raman spectrum in BP as stated in section for Raman measurement in text. Thus, we have employed the etching condition similar to that for formation of GNM. Then, Tc annealing was also carried out. Indeed, this resulted in significant enhancement of the ferromagnetism (Figs. 2A and 2C) as well as the case of GNM. Thus, we judged that amount of the magnetic defects is extremely small also in BPNM.

During the fabrication process using a nanoporous alumina template as the etching mask, no magnetic tools were employed to avoid extrinsic magnetization (e.g., plastic tweezers have been used).

(5) Detaching the NPATs from BP substrates

After formation of the nanomesh on BPs, the NPAT mask was entirely dissolved by a H_3PO_4 solution or detached mechanically from the BPNMs in some cases. It left no contamination. Then, all residual nanomeshes multi-layer BP flakes (i.e., except for few-layer BPNMs), which existed under the NPAT, were entirely removed by the mechanical method (i.e, by plastic tweezers) one by one to measure the magnetization of only the few-layer BPNMs. After removing, the absence of the nanomesh multi-layer BP flakes was reconfirmed following the above-mentioned SM (3).

(6) Annealing methods at T_c for the pore edge reconstruction to zigzag

All the BPNMs fabricated through these processes were annealed at 300 °C in high vacuum (10^{-6} Torr) for approximately 0.5 h with keeping pumping of gas. When annealing was performed at T > 300 °C, the BP nanomeshes disappeared. Thus, this temperature can be critical temperature for atomic reconstruction of BPNRs existing at the interpore regions and also the pore edges. At least, two pore edges can become zigzag (Fig. 1E) via. this T_c annealing. Then, almost samples are exposed into the air atmosphere for oxidization, while for hydrogenation, some samples were placed in hydrogen gas by the field-emission-type radical CVD system under pressure > 1MPa for at least 3 hours.

(7) Oxidation process

Basically, there is no other process for air exposure of the BPNMs except for this. We have mechanically exfoliated the BP samples and attached porous alumina template on it in the glove box in high vacuum. Then, we have carried the samples into the Ar gas etching facility by using a vacuum box. After the etching by Ar gas and formation of BPNMs, the BPNMs have been exposed in air as we mentioned in text and, then, the BPNM substrate has been cut into smaller parts in glove box. Finally, the oxidized BPNMs are placed into a SQUID and magnetization has been measured.

(8) Raman spectrum for P=O stretching mode

Figure 4S shows Raman spectrum of a ferromagnetic BP nanomesh in high-frequency region. The peaks observable around 1350 cm^{-1} correspond to P=O stretching mode. Development of how to make an

accurate estimate of oxygen concentration, which produces the present edge magnetism, will be indispensable based on this result.
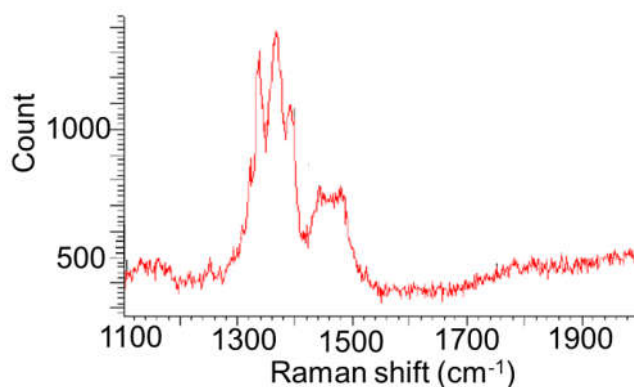

Fig. S4: Raman spectrum of a ferromagnetic BP nanomesh, showing P=O bond stretching mode around 1350 cm^{-1}.

(9) Possible contribution of electron-doped arm chair edge to edge magnetism

On the other hand, other calculation has reported presence of flat bands even in O-terminated arm chair PNRs in contradiction to the case of GNRs (9). Although the Fermi energy is located at approximately 1 eV below the flat band due to hole doing in it, it may also contribute to the observed ferromagnetism in BPNMs if electrons are doped from the substrate or as the result of band bending because of the presence of a mixture of zigzag and armchair pore edges.

(10) Unresolved problem

The present observations of the magnetization in BPNMs remain still incomprehensible in some samples. For instance, at temperatures above 320 K, the magnetization value anomalously increased with increasing temperature. It also exhibited hysteresis with a decrease and increase in a temperature (Fig.S4).

Conventionally, such a magnetization minimum has been observed for appearance of new another phase in magnetic materials. Moreover, interaction of localized single spin with free spin yielded it like the case of Kondo singlet, although Kondo temperature is very low. The discussed origin of the observed edge magnetism was single spin existing at unsaturated p_z bond in the edge P-O atoms. This unpaired spin may contribute to these unresolved problems. Further study is needed to reveal the origins of these behaviors, as is direct observation of the electronic structures of the pore edges.
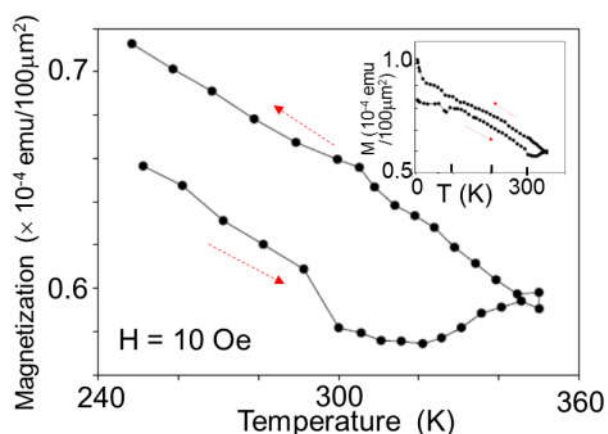

Fig.S4: Temperature dependence of the M_s values for the FM-BPNM at T > 240 K. Inset: for the temperature range 2 K < T < 350 K. When temperature increases, M_s values decreases monotonically. In contrast, it starts to increase above 320K anomalously. On the other hand, as temperature decreases, M_s values increase monotonically with showing a hysteresis. Arrows in figure mean a decrease and increase in temperatures.

(11) Estimation of edge magnetism

Magnetic moment per one dangling bond terminated by O atom in zigzag edge of the hexagonal pore is estimated as follows.

(1) The typical total area of BPNMs is ~0.4 cm^2.

(2) The area of one hexagonal unit cell with a pore is S = $6(3^{-1/2}/2)(a/2)^2$~4300 nm^2, where a = [80 nm (pore

diameter) + 20 nm (pore spacing)].

(3) Thus, the total number of pores is (0.4 cm²)/ (4300 nm²)~10^{12} [i.e., (1)/(2)].

(4) The total number of dangling bonds per hexagonal pore is (40 nm)/(0.216 nm × $3^{1/2}$) × 6 = 130 × 6 ~ 1000.

(5) The total number of edge dangling bonds of the mono-layer BPNM used for the SQUID measurement is ~10^{15} [(3) × (4)].

(6) The saturation magnetization per edge dangling bond is ~1 × 10^{-4} (emu) × 10^{-3}/[(10^{15} × 10 (layers)] = 1 × 10^{-23} (J/T).

(7) Thus, the magnetic moment per edge dangling bond is (1 × 10^{-23})/ (μ_B = 9.3 × 10^{-24}) ~ 1.0 μ_B, where μ_B is the Bohr magneton. This value is in good agreement with calculation result of the magnetization value of edge P=O bond explained in theoretical part of the manuscript (i.e., 0.95 μ_B = ($|M_P|$ = 0.55 μ_B)+($|M_O|$ = 0.4 μ_B)).

(12) Calculation method for edge magnetism

We have carried out first principles calculations in order to get some insight on the origins of the huge magnetism observed in oxidized few-layer BPNMs. For this aim, we have used the plane wave based PWSCF code, which is part of the QUANTUM-ESPRESSO [1] *ab initio* package. We focus on single layer O-terminated ZPNRs. The calculations were performed using the Perdew-Burke-Ernzerhof (PBE) exchange-correlation functional and projector-augmented wave (PAW) pseudopotentials to account for the core electrons. The kinetic energy cutoff was set to 40 Ry and a 30x1x1 Monkhorst-Pack *k*-point mesh was used for the self-consistent calculation. The geometries have been optimized by using the quasi-Newton Broyden-Fletcher-Goldfarb-Shanno (BGFS) algorithm as implemented in the PWSCF code. The relaxed geometries are shown in Fig. S5(a).

We also reveal that at the X-point the spin densities from the valence bands are only localized along the edges of the NR which strongly contributes to the edge-AFM state shown in Fig. S5(b). Magnetic PNRs become semiconductors due to Coulomb exchange interactions between electrons in the midgap states and the bands are spin degenerates. In Fig. S5(b), we have plotted the spin-density contribution of the valence band states $|\Psi^{\uparrow}_{VB}|^2$ and $|\Psi^{\downarrow}_{VB}|$ at Γ and X (note that because of the two valence bands are degenerate at X, we plot the density contribution of both bands VB and VB'). At the Γ-point, the up and down spin densities appear distributed across the NR. However, by summing both spin contributions, the spin densities in the interior of the NR cancel and only the ones centered at the P_{edge} and O atoms remain finite. In contrast, at the X-point the spin densities from the valence bands are only localized along the edges of the NR which strongly contributes to the edge-AFM state.
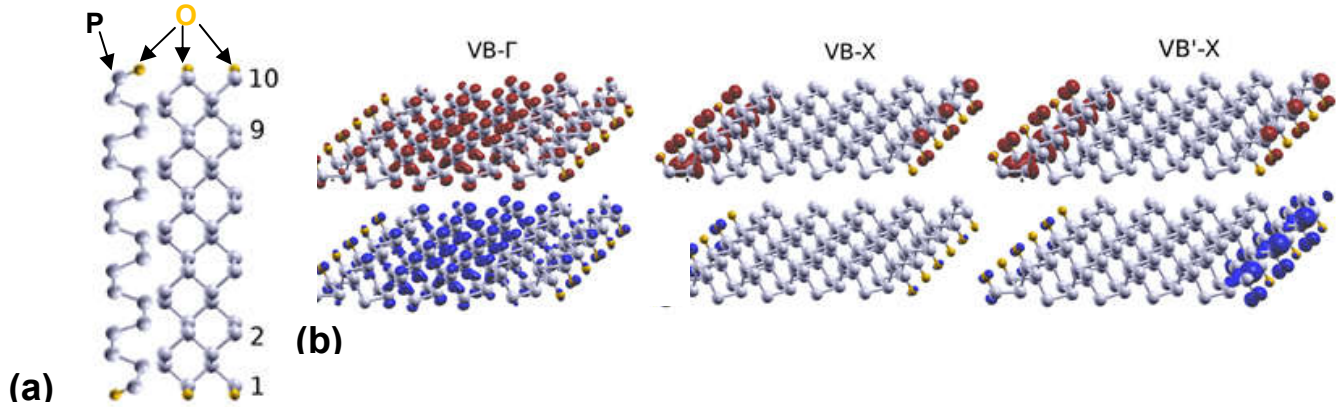

Fig. S5: **(a)** Optimized O-terminated (shown in yellow) 10-ZPNR geometries obtained by applying the BGFS algorithm as implemented in the PWSCF code. That corresponds to O-terminated interpore ZPNR region of BPNM shown in Fig. 1E. Distances are very similar to those reported for mono-layer PNR. The distance

between P and O atoms at the edges is 1.5 Å, which corresponds to a P=0 double bond. **(b)** Spin density contribution of the valence band state (labeled as VB). Red and blue colors are used for up and down spin densities, respectively. In both points of the Brillouin zone (Γ and X), the sum of spin contributions lead to spin polarized edges with e-AFM configuration. However, the main contribution to the spin polarization of the edges comes from the X-point where both valence bands (VB and VB') are degenerated.

Based on the calculation for the O-terminated mono-layer ZPNR, in order to understand the scaling of the magnetization with sample thickness d (Fig.3B; i.e., interlayer spin interaction), we have calculated magnetization vs. layer number (Fig. 6E), using the O-terminated 6-ZPNR. We focus on AB layer stacking since it shows lower ground state energy and is well known in BP as mentioned above. In the trilayer case, we have used an ABA stacking. First, we have relaxed the interlayer distance for both cases leading to $d_z \approx$ 0.198 nm. This is around 0.1 nm shorter than previously reported values for BP. This difference is due to the presence of O atom, which has some tendency to form new bonds with the neighboring layers, and to the lower dimensional character of the nanoribbon compared with bulk BP. This is consistent with previous reports which suggested that strong interlayer interaction in BP is not merely of vdW. We also find that presence of the edge O-atom also prevents appearance of Peierls transition. For the calculation of bilayer and trilayer O-terminated ZPNRs we have used the PBE-D2 which add the van der Waals energy dispersion to the PBE functional during geometry relaxation. This method has demonstrated to give good values of the interlayer distance in previous calculations on BP [2].

[1] P. Giannozzi, S. Baroni, N. Bonini, M. Calandra, R. Car, C. Cavazzoni, D. Ceresoli, G. L. Chiarotti, M. Cococcioni, I. Dabo, A. Dal Corso, S. Fabris, G. Fratesi, S. de Gironcoli, R. Gebauer, U. Gerstmann, C. Gougoussis, A. Kokalj, M. Lazzeri, L. Martin-Samos, N. Marzari, F. Mauri, R. Mazzarello, S. Paolini, A. Pasquarello, L. Paulatto, C. Sbraccia, S. Scandolo, G. Sclauzero, A. P. Seitsonen, A. Smogunov, P. Umari, R. M. Wentzcovitch, *J. Phys.: Condens. Matter* **21**, 395502 (2009).

[2] X. Luo, X. Lu, G. K. W. Koon, A. H. Castro-Neto, B. Özyilmaz, Q. Xiong & S. Y. Quek, Nano Letters 15 3931-3938 (2015).